Dual Mode Coupling by Square Corner Cut in Resonators and Filters

Xiao-Peng Liang, *Student Member, IEEE,* Kawthar A. Zaki, *Fellow, IEEE,* and Ali E. Atia, *Fellow, IEEE*

Abstract—**A new method for realization of dual mode coupling in rectangular waveguide cavities is described and analyzed. The method completely replaces the coupling screw, and therefore can be used to eliminate the need for tuning in dual mode waveguide cavity filters. It also offers a wide range of coupling values and can achieve higher power handling capability than coupling screws. Mode matching method is used to calculate the mode chart of the infinitely long square corner cut rectangular waveguide (SCCRW), the field distributions of each mode, and the resonant frequencies of the cavity. Evanescent mode rectangular waveguide is used to provide dual mode couplings between adjacent cavities. The junction discontinuity between the SCCRW and the rectangular waveguide is modeled by double mode matching method, obtaining modal scattering parameters of the junction. A 4-pole dual mode elliptic function rectangular waveguide cavity filter using the new coupling method was constructed. The natural frequencies of the whole filter structure is calculated and is verified by measurements. The experimental filter results showed excellent agreement with theory.**

I. Introduction

DUAL mode empty or dielectric loaded resonator filters are widely used in satellite communications, due to their higher selectivity, smaller size and less mass than conventional single mode direct coupled filters [1]–[7]. The usual way to couple dual modes is by adding a coupling screw at 45° angle with the direction of the electric fields of the two dual modes. By changing the coupling screw penetration in the cavity, the coupling between the two dual modes can be adjusted. Due to the sharpness of the coupling screws, the filter's power handling capability is reduced. Although the tuning and the coupling screws provide flexibility for adjusting the filter's response, the tuning process itself is time consuming and makes the cost of dual mode filters production high. Waveguide components can be miniaturized by filling them with high dielectric constant material, resulting in linear dimensions reduction by a factor of $1/\sqrt{\epsilon_r}$ [8]. Completely removing screws from dual mode filters is the first step toward this miniaturization. Recently, a method has been introduced to realize dual mode coupling in planar waveguide structures [7]. The realization is through a perturbation of the single mode microstrip line resonator. On waveguide structures, a similar method can be used to replace the coupling screws in dual mode filters. This paper introduces and analyzes such a method, which provides a square corner cut in rectangular waveguide cavity, as shown in Fig. 1(a). The new mechanism has the ability to provide a wide range of coupling values with minor reduction of cavity power handling capability and the potential of reducing production cost of dual mode waveguide and dielectric filled cavity filters by eliminating the need for tuning altogether. The key is the ability to accurately analyze the coupling configuration.

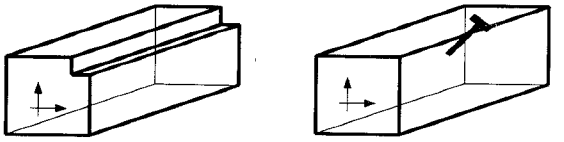

(a) (b)

Fig. 1. Coupling configurations (a) new method, and (b) conventional coupling screw.

To illustrate the application of the new coupling mechanism, an experimental 4-pole dual mode elliptic function rectangular waveguide cavity filter was designed. In reference [6] a length of evanescent mode rectangular waveguide was used to provide the required coupling values between physically adjacent cavities and is accurately modeled by mode matching method. These couplings can be separately controlled by the two dimensions in the cross section. The same method is used in the present paper to design the 4-pole dual mode filter.

The square corner cut rectangular waveguide (SCCRW) is modeled by mode matching method, producing the mode chart of the infinitely long waveguide, the field distribution of each mode, and the resonant frequencies of the cavity. The junction discontinuity between SCCRW and evanescent mode rectangular waveguide is also modeled by mode matching, yielding modal scattering parameters of the junction and then the natural frequencies of the 4-pole dual mode filter structure, including all the couplings.

The numerical results are verified by measurements. The experimental filter was tested, showing excellent agreement with theory, with no tuning.

II. Theoretical Analyses

A. Square Corner Cut Rectangular Waveguide

Fig. 1(a) shows the proposed new coupling configuration under study. A square (or rectangular) waveguide

Manuscript received March 31, 1992; revised August 3, 1992.

X.-P. Liang and K. A. Zaki are with the Electrical Engineering Department, University of Maryland, College Park, MD 20742.

A. E. Atia is with COMSAT System Division, 22300 Comsat Drive, Clarksburg, MD 20871.

IEEE Log Number 9203704.

cavity is perturbed by a square cut on one of its corners. With no cut, the square waveguide cavity has two dominant degenerate modes with the same resonant frequencies and perpendicular electric field distributions. Those two modes can be referred to as TE_{101} and TE_{011} modes and are decoupled from each other. With the square cut, the two dominant modes will be coupled to each other, and the resonant frequencies will split. As a comparison, the conventional method of coupling the two dual modes in a cavity by a coupling screw is shown in Fig. 1(b).

To analyze the SCCRW cavity, first, the infinitely long perfectly conducting SCCRW, with the cross section shown in Fig. 2, is analyzed. Mode matching method is employed to solve this problem. The cross section is divided into two regions. Region I is the area $0 \le y \le b_1$, and region II is the area $b_1 \le y \le b_2$. The modes existing in the SCCRW are still TE and TM modes [9].

1. TE modes

For region I,

$$j\omega\mu H_{z1} = \sum_n D_{1n} \cos(k_{x1n}x) \cosh(k_{y1n}y) \tag{1a}$$

$$E_{x1} = -\sum_n \frac{D_{1n}}{k_c^2} k_{y1n} \cos(k_{x1n}x) \sinh(k_{y1n}y) = Z_{TE} H_{y1} \tag{1b}$$

$$E_{y1} = -\sum_n \frac{D_{1n}}{k_c^2} k_{x1n} \sin(k_{x1n}x) \cosh(k_{y1n}y) = -Z_{TE} H_{x1} \tag{1c}$$

where

$$k_{x1n}^2 - k_{y1n}^2 = \gamma^2 + k^2 = k_c^2 \tag{1d}$$

$$k_{x1n} = \frac{n\pi}{a_2},\ k^2 = \omega^2\mu\epsilon,\ Z_{TE} = \frac{j\omega\mu}{\gamma} \tag{1e}$$

γ, k_c, and Z_{TE} are the propagation constant, the cut-off wave number, and the wave impedance, respectively.

For region II,

$$j\omega\mu H_{z2} = \sum_m D_{2m} \cos(k_{x2m}x) \cosh(k_{y2m}(y - b_2)) \tag{2a}$$

$$E_{x2} = -\sum_m \frac{D_{2m}}{k_c^2} k_{y2m} \cos(k_{x2m}x) \sinh(k_{y2m}(y - b_2)) = Z_{TE} H_{y2} \tag{2b}$$

$$E_{y2} = -\sum_m \frac{D_{2m}}{k_c^2} k_{x2m} \sin(k_{x2m}x) \cosh(k_{y2m}(y - b_2)) = -Z_{TE} H_{x2} \tag{2c}$$

where

$$k_{x2m}^2 - k_{y2m}^2 = \gamma^2 + k^2 = k_c^2 \tag{2d}$$

$$k_{x2m} = \frac{m\pi}{a_1} \tag{2e}$$

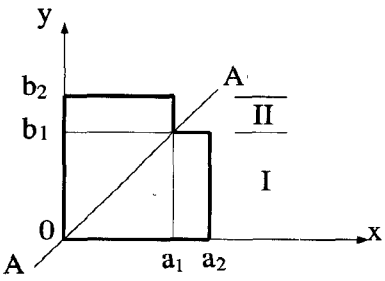

Fig. 2. Coordinate system and the cross section of the SCCRW.

By applying the boundary conditions at $y = b_1$, taking the inner products, and using the orthogonality relations on the sinusoidal functions in each region, the following characteristic equation is obtained:

$$\det[X] = 0 \tag{3}$$

where X is an $(N \times N)$ matrix and N is the number of eigen-modes used in region I. The elements of the matrix X are

$$x_{ij} = \cosh(k_{y1j}b_1) \sum_{m=0}^{M} [T_m k_{y2m} \tanh(k_{y2m}(b_1 - b_2)) \cdot \langle \hat{e}_{2m}, \hat{h}_{1j} \rangle \langle \hat{e}_{2m}, \hat{h}_{1i} \rangle] - \delta_{ij} \frac{a_1 a_2}{4T_i} k_{y1i} \sinh(k_{y1i}b_1) \tag{4a}$$

$$T_m = \begin{cases} 1, & m \neq 0 \\ \frac{1}{2}, & m = 0, \end{cases},\ \delta_{ij} = \begin{cases} 0, & i \neq j \\ 1, & i = j \end{cases} \tag{4b}$$

where $(M + 1)$ is the number of modes used in region II. And the inner product of $\langle \hat{e}, \hat{h} \rangle$ are simply the line integrations of two multiplied sinusoidal functions in x direction at $y = b_1$.

Solving (3), a group of eigen-values of γ's can be obtained. Each γ corresponds to a mode in the SCCRW.

2. TM modes

Similar procedures can be used to describe TM waves in the SCCRW. The same characteristic equation as equation (3) is obtained with the matrix elements given by

$$x_{ij} = \cosh(k_{y1j}b_1) \sum_{m=1}^{M} \left[\frac{\tanh(k_{y2m}(b_1 - b_2))}{k_{y2m}} \cdot \langle \hat{e}_{2m}, \hat{h}_{1j} \rangle \langle \hat{e}_{2m}, \hat{h}_{1i} \rangle \right] - \delta_{ij} \frac{a_1 a_2}{4} \frac{\sinh(k_{y1i}b_1)}{k_{y1i}} \tag{5}$$

And the wave impedance is

$$Z_{TM} = -\frac{j\omega\mu\gamma}{k^2} \tag{6}$$

A computer program using the mode matching technique was developed to calculate the propagation constants for the modes that can exist in the waveguide. Fig.

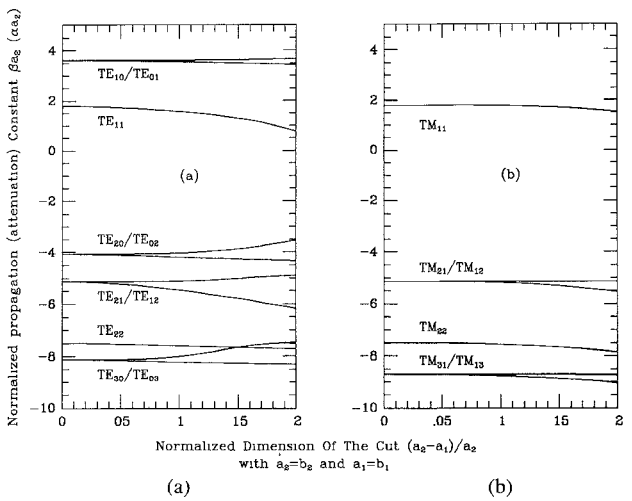

Fig. 3. Mode charts of the SCCRW with (a) TE, and (b) TM modes.

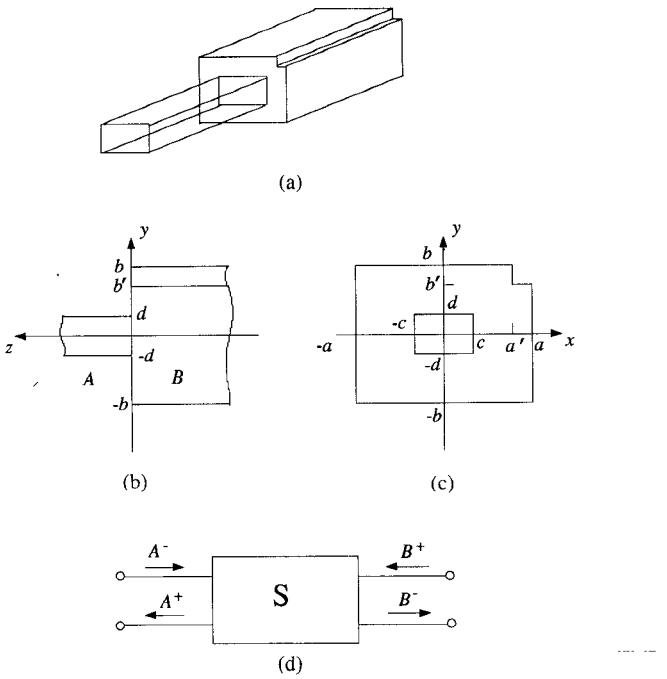

Fig. 4. Junction discontinuity between SCCRW and rectangular waveguide with (a) configuration, (b) and (c) coordinate system, and (d) equivalent scattering parameter network.

3 shows the variation of the normalized propagation constants with the normalized size of the square cut for several TE and TM modes at normalized frequency $fa_2 = 9$ GHz · inch (i.e. $(a_2/\lambda_0) = 0.762$). The normalized propagation constants βa_2 for propagating modes are shown as positive, and the attenuation constants αa_2 of cut-off modes are shown as negative. The split of the dual modes (i.e. TE_{10}/TE_{01}, TE_{20}/TE_{02}, TE_{21}/TE_{12} and TE_{30}/TE_{03} in Fig. 3(a)) is clearly apparent when the dimension of the square cut increases. Due to the different propagation constants of all the dual modes, once the two conducting short circuit planes are added to form a waveguide cavity, the corresponding resonant frequencies for the dual modes will also be different.

B. Junction of SCCRW's And Rectangular Waveguides

Evanscent mode rectangular waveguide can be used to provide dual mode couplings between physical adjacent cavities. The junction discontinuity between SCCRW and rectangular waveguide, as shown in Fig. 4(a), can be modeled by using mode matching method twice. First mode matching method is used to find the modes existing in SCCRW. Second mode matching is again used to solve the discontinuity problem to obtain modal scattering parameters.

The junction discontinuity shown in Fig. 4 is divided into two regions. The rectangular waveguide side is region A, and the SCCRW side is region B. The transverse fields in each region can be expressed in terms of incident and reflected waves [10]:
For region A,

$$\bar{E}_{tA} = \sum_{i=1}^{N} [A_i^+ e^{-\gamma_{Ai}z} + A_i^- e^{\gamma_{Ai}z}]\hat{e}_{Ai} \tag{7a}$$

$$\bar{H}_{tA} = \sum_{i=1}^{N} [A_i^+ e^{-\gamma_{Ai}z} - A_i^- e^{\gamma_{Ai}z}]\hat{h}_{Ai} \tag{7b}$$

where $\hat{e}_{Ai}$ and $\hat{h}_{Ai}$ are the normal modes electric and magnetic fields, respectively; γ_{Ai} is the propagation constant of each mode; and N is the number of modes, including both TE and TM modes. Coefficients A_i^- are the incident waves from $z < 0$ to the junction, and A_i^+ are the reflected waves from the junction.
Similarly, for region B,

$$\bar{E}_{tB} = \sum_{j=1}^{M} [B_j^+ e^{-\gamma_{Bj}z} + B_j^- e^{\gamma_{Bj}z}]\hat{e}_{Bj} \tag{8a}$$

$$\bar{H}_{tB} = \sum_{j=1}^{M} [B_j^+ e^{-\gamma_{Bj}z} - B_j^- e^{\gamma_{Bj}z}]\hat{h}_{Bj} \tag{8b}$$

where M is the number of modes (TE and TM), and B_j^+ and B_j^- are the incident and reflected waves, respectively. The relationships among A_i^+, A_i^-, B_j^+, and B_j^- can be described by a multiport generalized modal scattering network, as shown in Fig. 4(d) [10].

Matching the boundary conditions at $z = 0$, which require the tangential fields to be continuous, and taking the inner products with orthogonality relations of modes in each region taken into account, the following relation can be obtained:

$$\begin{bmatrix} A^+ \\ B^- \end{bmatrix} = \begin{bmatrix} P_{11} & P_{12} \\ P_{21} & P_{22} \end{bmatrix}^{-1} \begin{bmatrix} -P_{11} & -P_{12} \\ P_{21} & P_{22} \end{bmatrix} \begin{bmatrix} A^- \\ B^+ \end{bmatrix} = \begin{bmatrix} S_{11} & S_{12} \\ S_{21} & S_{22} \end{bmatrix} \begin{bmatrix} A^- \\ B^+ \end{bmatrix} \tag{9}$$

where the submatrices P_{11}, P_{12}, P_{21} and P_{22} have the orders $M \times N$, $M \times M$, $N \times N$ and $N \times M$, respectively. The elements of each submatrix are given in Appendix.

The modal scattering parameter submatrices of S_{11}, S_{12}, S_{21} and S_{22} have orders $N \times N$. $N \times M$, $M \times N$ and $M \times M$, respectively. Exchanging region A and B in Fig. 4(a) simply requires the exchanges of S_{11} with S_{22} and S_{12} with S_{21}, respectively, in (9). For faster convergence in numerical calculation, the ratio of N/M should be proportional to the ratio of the cross section areas of region A and region B.

Compared with scattering parameters, the generalized modal scattering parameters given above have somewhat different properties which can be summarized by the following:

1) Normal scattering parameters relate incident and reflected propagating modes in a transmission line. Modal scattering parameters relate the waves in a waveguide, including both propagating and evanescent waves.
2) Normal scattering parameters are normalized by input and output powers. There is no physical meaning for power in evanescent waves in a waveguide. Even using the word "wave" is not suitable for evanescent modes, because there is no real "waves" for evanescent modes. To be consistent with the propagating waves, "evanescent wave" is still used here for simplicity.
3) If only one propagating wave exists in a waveguide, then unitary and reciprocal properties are valid only for this propagating wave in the modal scattering parameters.
4) Normalization of modal scattering parameters is made by multiplication with the corresponding inner products $\langle \hat{e}_i, \hat{h}_i^* \rangle$ of each mode to the field coefficients. The relation between unnormalized (S_{ij}) and normalized (S_{ij}^n) modal scattering parameters are

$$S_{ij}^n = S_{ij} \left| \sqrt{\frac{\langle \hat{e}_i, \hat{h}_i^* \rangle}{\langle \hat{e}_j, \hat{h}_j^* \rangle}} \right|. \tag{10}$$

The inner products represent powers only for propagating waves, in which case they are positive numbers. However, they become purely imaginary numbers for evanescent waves [9]. In order to avoid the sign ambiguities when taking square root of a pure imaginary number, absolute values have to be taken in (10).

III. Dual Mode Coupling

A. In A Cavity

The two equivalent circuits shown in Fig. 5 can be used to model the coupling structures between two single mode cavities [4]–[6]. If the coupling coefficient between the cavities is M, then from the symmetry of the structure, it is possible to calculate M from a knowledge of the resonant frequencies f_e and f_m, where f_e and f_m are the resonant frequencies assuming the symmetric plane A − A as a perfect electric conductor and a perfect magnetic conductor, respectively. The coupling coefficient is simply:

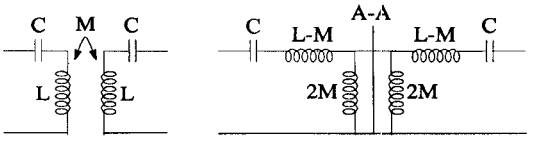

Fig. 5. Equivalent circuits of the coupling in one physical cavity.

$$c = \frac{M}{L} = \frac{f_e^2 - f_m^2}{f_e^2 + f_m^2}. \tag{11}$$

The field distribution in the cross section for the first dual modes in the SCCRW are calculated and plotted in Fig. 6(a) and (b). From these two plots, it is seen that the plane perpendicular to the cross section, containing the z-axis and the line parallel to the z-axis through the vertex of the square cut (a_1, b_1) in the cross section is the symmetric plane A − A as marked in Fig. 2. The electric fields at this plane are maximum and are parallel to the plane for the odd modes (magnetic wall) and perpendicular to the plane for the even modes (electric wall). These two modes are just the split dual modes due to square cut perturbation. Equation (11) can be used to calculate the coupling coefficient, where f_e and f_m are the two split resonant frequencies with the higher one as f_e (smaller propagation constant, electric wall) and lower one as f_m (larger propagation constant, magnetic wall).

B. In A 4-Pole Filter

A 4-pole dual mode filter configuration is shown in Fig. 7(a), which uses the new mechanism to provide dual mode coupling in one physical cavity and the evanescent mode rectangular waveguide to provide dual mode couplings between two physical cavities. The corresponding modal scattering parameter network is given in Fig. 7(b), where the two modal scattering parameter networks S^I and S^{II} represent the two junction discontinuities between SCCRW and rectangular waveguide. The two square corner cuts are at different corners in the two cavities to produce the necessary negative M_{14} coupling for elliptic filter response. By cascading the two networks [10] with the three waveguide lengths, a simplified network can be obtained, as shown in Fig. 7(c). If two short circuits are introduced at the input/output ports, the natural frequencies of the configuration can be obtained by solving the equation:

$$\det [S + I] = 0 \tag{12}$$

where I is a unit matrix.

An equivalent circuit of the 4-pole dual mode filter configuration in terms of coupling coefficients M_{ij} with short circuits at input/output ports is given in Fig. 8. From this equivalent circuit, the four natural frequencies can be calculated in terms of the coupling coefficients and the filter

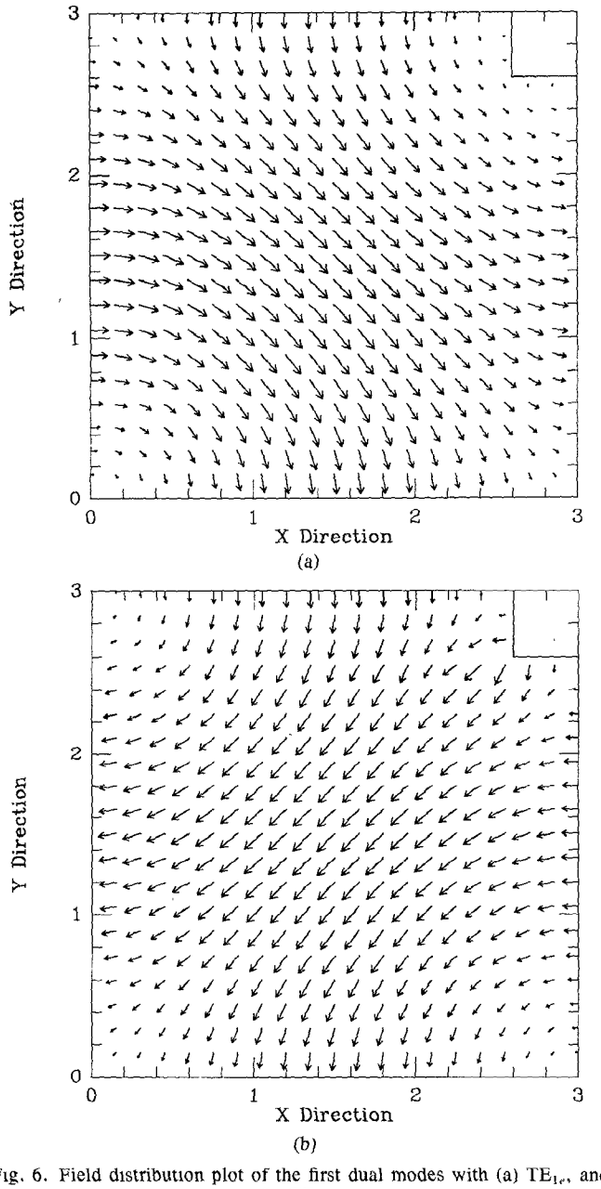

Fig. 6. Field distribution plot of the first dual modes with (a) TE_{1e}, and (b) TE_{1m}.

center frequency, as

$$f_1^2 = f_0^2 \cdot \frac{2 + m_{14} + m_{23} - \sqrt{(m_{14} - m_{23})^2 + 4m_{12}^2}}{2[(1 + m_{14})(1 + m_{23}) - m_{12}^2]} \tag{13a}$$

$$f_2^2 = f_0^2 \cdot \frac{2 + m_{14} + m_{23} + \sqrt{(m_{14} - m_{23})^2 + 4m_{12}^2}}{2[(1 + m_{14})(1 + m_{23}) - m_{12}^2]} \tag{13b}$$

$$f_3^2 = f_0^2 \cdot \frac{2 - m_{14} - m_{23} - \sqrt{(m_{14} - m_{23})^2 + 4m_{12}^2}}{2[(1 - m_{14})(1 - m_{23}) - m_{12}^2]} \tag{13c}$$

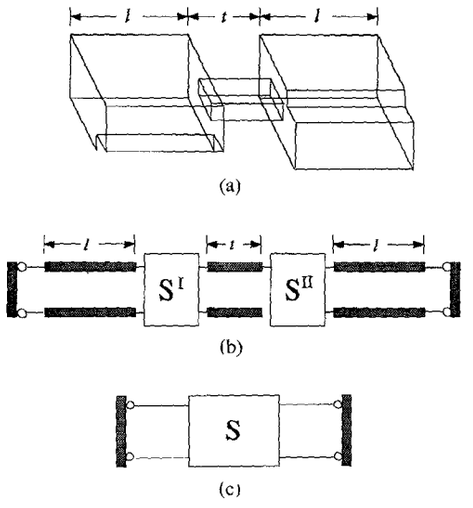

Fig. 7. 4-pole dual mode filter configuration with (a) configuration, (b) equivalent scattering parameter network, and (c) simplified scattering parameter network.

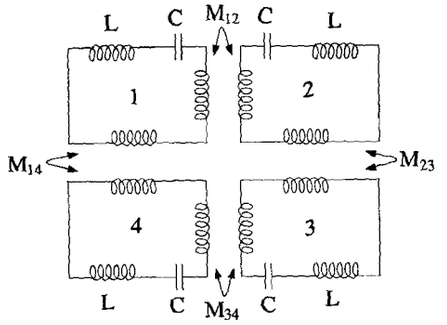

Fig. 8. Equivalent circuit of a 4-pole dual mode filter structure.

$$f_4^2 = f_0^2 \cdot \frac{2 - m_{14} - m_{23} + \sqrt{(m_{14} - m_{23})^2 + 4m_{12}^2}}{2[(1 - m_{14})(1 - m_{23}) - m_{12}^2]} \tag{13d}$$

where

$$m_{ij} = \frac{M_{ij}}{L}, f_0 = \frac{1}{2\pi\sqrt{LC}}, m_{34} = m_{12}. \tag{14}$$

If the coupling coefficients m_{ij} and the filter center frequency f_0 are given (e.g. from a synthesis procedure [1]), the four desired natural frequencies can be calculated from (13). These four natural frequencies must also be solutions of (12). Thus the filter structure dimensions are related to the synthesized coupling values, through the natural frequencies. Several iterations on the various dimensions can be made to produce the required natural frequency values of the filter structure with acceptable accuracies. Equation (11) gives initial value of the desired cut dimension to provide M_{12} by square corner cut in SCCRW. However, when the effects of the other couplings are introduced through (13), the cut dimensions need further adjustment, due to the interactions of all the

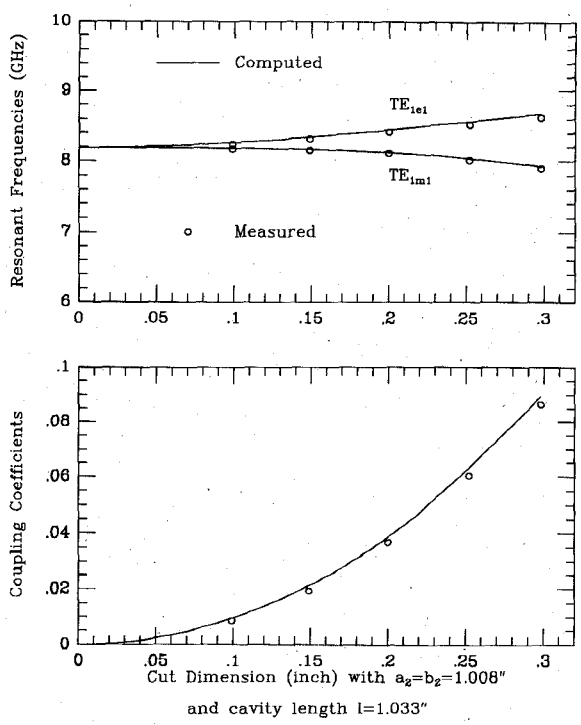

Fig. 9. Comparison of computed and measured f_e, f_m, and c for a SCCRW cavity resonator.

couplings. Usually, a 4-pole dual mode elliptic function filter requires $|m_{14}| \neq |m_{23}|$, thus the dimensions of the evanescent mode rectangular waveguide c and d must be different. This difference produces different loading effects on the center frequencies of each electrical resonator [11]. To keep the same center frequencies of each resonator, the SCCRW cavity dimensions a and b will also be slightly different.

IV. Numerical and Experimental Results

A computer program was developed to compute the propagation constants for each mode in the SCCRW, its field distribution, f_e, f_m, and c of (11). Fig. 9 shows the calculated and measured results for TE_{10}/TE_{01} modes in an experimental cavity resonator.

A computer program for obtaining the modal scattering parameters of the junction between SCCRW and rectangular waveguide and then solving equation (12) for the natural frequencies was also developed. The four natural frequencies are calculated as functions of the dimensions of the 4-pole dual mode filter configuration in Fig. 7(a). Fig. 10(a)–(e) gives the typical numerical results and Fig. 10(f) gives the measured data. The cross section dimensions definitions are given in Fig. 4. Fig. 10 can be used as filter design charts. The effects of placing the square corner cut at the same relative position in the two cavities (i.e. M_{14} positive) on the natural frequencies is shown in Fig. 11. Comparing Figs. 10(f) and (11), it is clear that completely different natural frequencies are obtained, and that the variation trends with the evanescent waveguide length are also different.

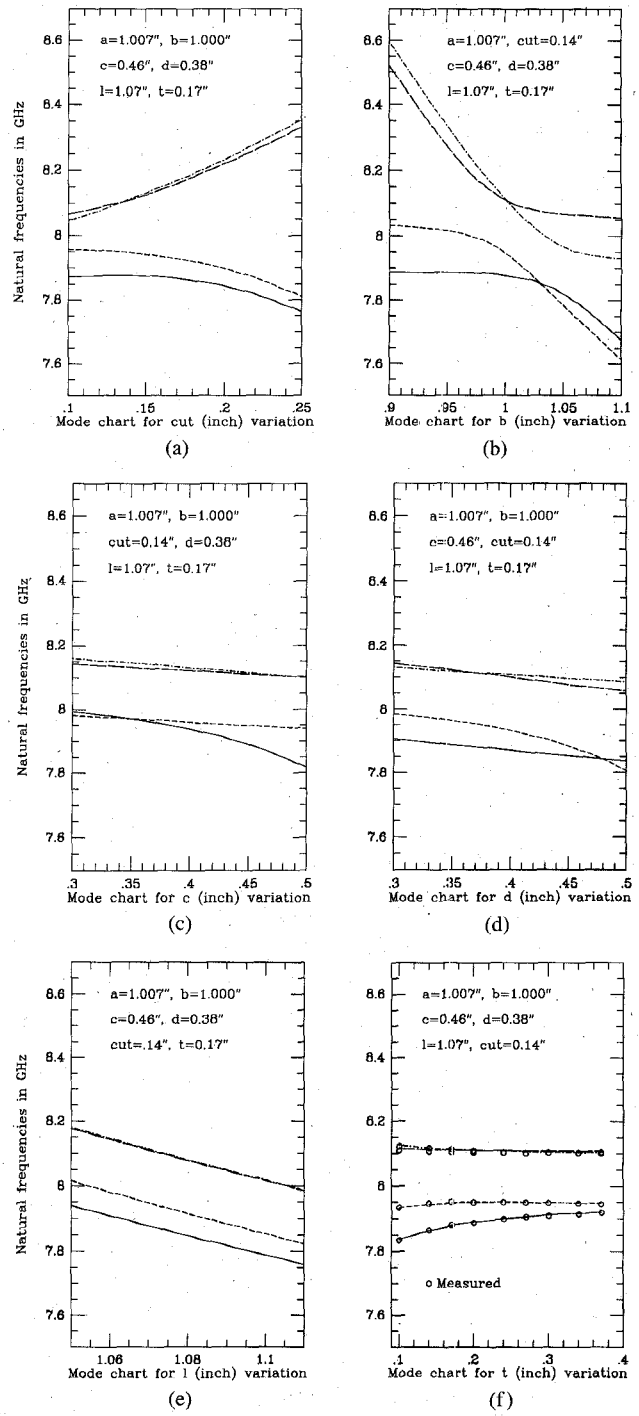

Fig. 10. Design charts of a 4-pole dual mode filter structure in terms of natural frequencies (cut = $a - a' = b - b'$).

In order to verify the usefulness and validity of the new coupling method, a C-band 4-pole dual mode filter using the new technique was designed. The coupling between dual modes in the cavities are $m_{12} = m_{34} = c = 0.01628$, which are provided by the cut in each cavity. The coupling through the evanescent mode rectangular hole are $m_{14} = -0.00603$, and $m_{23} = 0.01622$, which are controlled by the dimensions of the hole. The measured filter responses are shown in Fig. 12. These results agree closely with the theoretical filter responses.

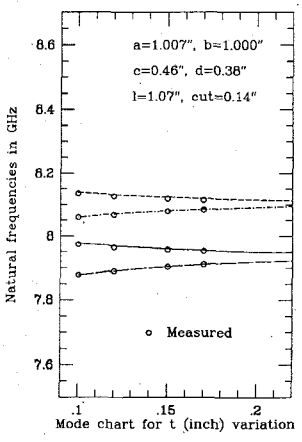

Fig. 11. Comparison with Fig. 10(f) at the same structure, except the two corner cuts being relatively at the same corner in the two physical cavities.

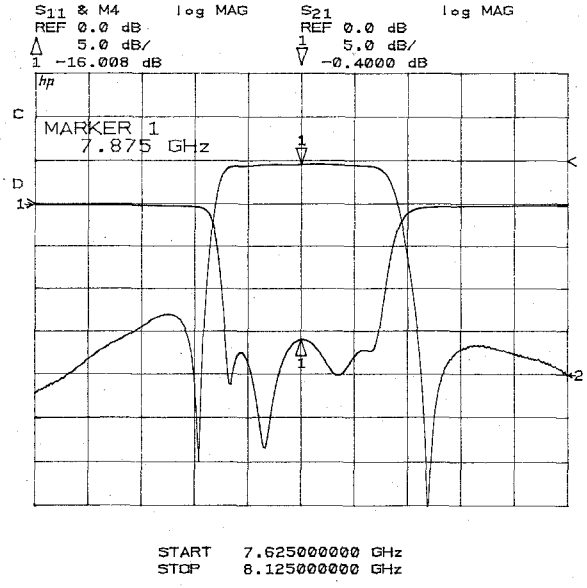

Fig. 12. Measured responses of a 4-pole dual mode filter.

V. Conclusions

The new dual mode coupling mechanism presented in this paper is simple, reliable, and flexible. It allows a wide range of variation of the coupling with a reasonable cut dimension. The same strategy can be used to couple dielectric loaded resonator dual mode filters. Mode matching method was successfully applied to accurately compute the propagation constants of the waveguide and then the resonant frequencies and the couplings of the dual mode cavity. Double mode matching was used to model the junction discontinuity between SCCRW and rectangular waveguide, producing modal scattering parameters. Scattering parameter network model of dual mode filter structure was given, calculating the natural frequencies of the structure. Dual mode filter design charts based on the natural frequencies of the filter structure were provided. Experimental verification of the calculated results were performed. Finally, a 4-pole dual mode filter was designed using the new coupling mechanism. Measurements on the filter show the validity of the method. This configuration has the potential for relatively inexpensive production of dual mode microwave and millimeter wave filters, since the cavities can be easily machined (e.g. using Numerical Controlled Mill), then assembled to give the required response with no tuning. It also provides the possibilities of miniaturization, by using the same configuration in a dielectric filled filter.

Appendix

The elements of the submatrices of $P_{ij}(i, j = 1, 2)$ in (9) are inner products of $\langle \hat{e}, \hat{h}^* \rangle$, defined as

$$\langle \hat{e}, \hat{h}^* \rangle = \int_S \hat{e} \times \hat{h}^* \cdot \hat{a}_z dS \tag{A1}$$

where S is the waveguide cross section. These elements are given by

$$(p_{ij})_{11} = \langle \hat{e}_{Aj}, \hat{h}^*_{Bi} \rangle \tag{A2}$$

$$(p_{ij})_{12} = -\delta_{ij} \langle \hat{e}_{Bi}, \hat{h}^*_{Bj} \rangle \tag{A3}$$

$$(p_{ij})_{21} = \delta_{ij} \langle \hat{e}^*_{Ai}, \hat{h}_{Aj} \rangle \tag{A4}$$

$$(p_{ij})_{22} = \langle \hat{e}^*_{Ai}, \hat{h}_{Bj} \rangle. \tag{A5}$$

A. Self Inner Products In Region A

$$\langle \hat{e}_{Ai}, \hat{h}^*_{Ai} \rangle = \frac{\gamma_i^*}{-j\omega\mu k_{ci}^4} [k_{yi}^2 \overline{CSA} + k_{xi}^2 \overline{SCA}],$$

TE mode (A6-1)

$$= \frac{k^2 \gamma_i}{j\omega\mu k_{ci}^4} [k_{xi}^2 \overline{CSA} + k_{yi}^2 \overline{SCA}], \quad \text{TM mode}$$

(A6-2)

$$\overline{CSA} = \int_{-c}^{c} \cos^2 k_{xi}(x + c)\, dx \cdot \int_{-d}^{d} \sin^2 k_{yi}(y + d)\, dy \tag{A6-3}$$

$$\overline{SCA} = \int_{-c}^{c} \sin^2 k_{xi}(x + c)\, dx \cdot \int_{-d}^{d} \cos^2 k_{yi}(y + d)\, dy \tag{A6-4}$$

$$k_{ci}^2 = k_{xi}^2 + k_{yi}^2 = k^2 + \gamma_i^2 \tag{A6-5}$$

$$k^2 = \omega^2 \mu_0 \epsilon_0 \tag{A6-6}$$

where i denotes the number of modes.

B. Self Inner Products In Region B

$$\langle \hat{e}_{Bi}, \hat{h}^*_{Bi} \rangle = \frac{\gamma_i^*}{-j\omega\mu k_{ci}^4} \left\{ \sum_n D_{1ni}^2 [k_{y1n}^2 \overline{CSB} + k_{x1n}^2 \overline{SCB}_1] + \sum_n D_{2mi}^2 [k_{y2m}^2 \overline{CSB}_2 + k_{x2m}^2 \overline{SCB}_2] \right\},$$

TE mode (A7-1)

$$= \frac{k^2 \gamma_i}{j\omega\mu k_{ci}^4} \left\{ \sum_n D_{1ni}^2 \left[\frac{k_{x1n}^2}{k_{y1n}^2} \overline{CSB}_1 + \overline{SCB}_1 \right] + \sum_m D_{2mi}^2 \left[\frac{k_{x2m}^2}{k_{y2m}^2} \overline{CSB}_2 + \overline{SCB}_2 \right] \right\},$$

TM mode (A7-2)

$$\overline{CSB}_1 = \int_{-a}^{a} \cos^2 k_{x1n}(x + a)\, dx \cdot \int_{-b}^{b'} \sinh^2 k_{y1n}(y + b)\, dy \quad \text{(A7-3)}$$

$$\overline{SCB}_1 = \int_{-a}^{a} \sin^2 k_{x1n}(x + a)\, dx \cdot \int_{-b}^{b'} \cosh^2 k_{y1n}(y + b)\, dy \quad \text{(A7-4)}$$

$$\overline{CSB}_2 = \int_{-a}^{a'} \cos^2 k_{x2n}(x + a)\, dx \cdot \int_{b'}^{b} \sinh^2 k_{y2m}(y - b)\, dy \quad \text{(A7-5)}$$

$$\overline{SCB}_2 = \int_{-a}^{a'} \sin^2 k_{x2m}(x + a)\, dx \cdot \int_{b'}^{b} \cosh^2 k_{y2m}(y - b)\, dy \quad \text{(A7-6)}$$

where coefficients D's are given when solving (3) to find the modes in the SCCRW.

C. Mutual Inner Products

The filter configuration used and shown in Fig. 4 must satisfy: $c < a'$ and $d < b'$.

$$\langle \hat{e}_{Ai}, \hat{h}^*_{Bj} \rangle = \frac{\gamma_{Bj}^*}{j\omega\mu k_{cAi}^2 k_{cBj}^2} \sum_n D_{1nBj} [k_{yAi} k_{y1nBj}^2 \overline{CSAB} - k_{xAi} k_{x1nBj} \overline{SCAB}], \begin{Bmatrix} \text{TE in region A} \\ \text{TE in region B} \end{Bmatrix} \quad \text{(A8-1)}$$

$$= \frac{k^2}{-j\omega\mu k_{cAi}^2 k_{cBj}^2} \sum_n D_{1nBj} [k_{yAi} k_{x1nBj} \overline{CSAB} - k_{xAi} \overline{SCAB}], \begin{Bmatrix} \text{TE in region A} \\ \text{TM in region B} \end{Bmatrix} \quad \text{(A8-2)}$$

$$= \frac{\gamma_{Ai} \gamma_{Bj}^*}{-j\omega\mu k_{cAi}^2 k_{cBj}^2} \sum_n D_{1nBj} [k_{xAi} k_{y1nBj}^2 \overline{CSAB} + k_{yAi} k_{x1nBj} \overline{SCAB}], \begin{Bmatrix} \text{TM in region A} \\ \text{TE in region B} \end{Bmatrix} \quad \text{(A8-3)}$$

$$= \frac{\gamma_{Ai} k^2}{j\omega\mu k_{cAi}^2 k_{cBj}^2} \sum_n D_{1nBj} [k_{xAi} k_{x1nBj} \overline{CSAB} + k_{yAi} \overline{SCAB}], \begin{Bmatrix} \text{TM in region A} \\ \text{TM in region B} \end{Bmatrix} \quad \text{(A8-4)}$$

$$\overline{CSAB} = \int_{-c}^{c} \cos k_{xAi}(x + c) \cos k_{x1nBj}(x + a)\, dx \cdot \int_{-d}^{d} \sin k_{yAi}(y + d) \frac{\sinh k_{y1nBj}(y + b)}{k_{y1nBj}}\, dy \quad \text{(A8-5)}$$

$$\overline{SCAB} = \int_{-c}^{c} \sin k_{xAi}(x + c) \sin k_{x1nBj}(x + a)\, dx \cdot \int_{-d}^{d} \cos k_{yAi}(y + d) \frac{\cosh k_{y1nBj}(y + b)}{k_{y1nBj}}\, dy \quad \text{(A8-6)}$$

REFERENCES

[1] A. E. Atia and A. E. Williams, "New type of bandpass filters for satellite transponders," *COMSAT Technical Review*, vol. 1, no. 1, pp. 21–43, Fall 1971.

[2] A. E. Atia and A. E. Williams, "Narrow bandpass waveguide filters," *IEEE Trans. Microwave Theory Tech.* vol. MTT-20, pp. 258–265, Apr. 1972.

[3] S. J. Fiedziusko, "Dual-mode dielectric resonator loaded cavity filters," *IEEE Trans. Microwave Theory Tech.*, vol. MTT-30, pp. 1311–1316, Sept. 1982.

[4] K. A. Zaki, C. Chen, and A. E. Atia, "Canonical and longitudinal dual mode dielectric resonator filters without iris," *IEEE Trans. Microwave Theory Tech.*, vol. MTT-35, pp. 1130–1135, Dec. 1987.

[5] S.-W. Chen and K. A. Zaki, "A novel coupling method for dual-mode dielectric resonators and waveguide filters," *IEEE Trans. Microwave Theory Tech.*, vol. 38, pp. 1885–1893, Dec. 1990.

[6] H.-C. Chang and K. A Zaki, "Evanescent-mode coupling of dual-mode rectangular waveguide filters," *IEEE Trans. Microwave Theory Tech.*, vol. 39, pp. 1307–1312, Aug. 1991.

[7] J. A. Curtis and S. J. Fiedziusko, "Miniature dual mode microstrip filters," in *1991 IEEE MTT-S Int. Microwave Symp. Dig.*, vol. 2, pp. 443–446.

[8] Y. Konishi, "Novel dielectric waveguide components—microwave applications of new ceramic materials," *Proc. IEEE*, vol. 79, pp. 726–740, June 1991.

[9] R. E. Collin, *Field Theory of Guided Waves*. New York: McGraw-Hill, 1960, ch. 5, pp. 171–189.

[10] A. S. Omar and K. Schünemann, "Transmission matrix representation of finline discontinuities," *IEEE Trans. Microwave Theory Tech.*, vol. MTT-33, pp. 765–770, Sept. 1985.

[11] G. Matthaei, L. Young, and E. M. T. Jones, *Microwave Filters, Impedance-Matching Networks, and Coupling Structures*. New York: McGraw-Hill, 1964, ch. 8, pp. 434–438.

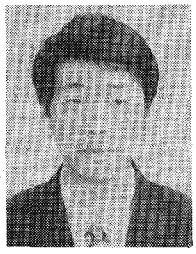

Xiao-Peng Liang (S'90) was born in Shanxi, China, in 1960. He received his B.S. and M.S. degrees in Beijing Institute of Technology, Beijing, China, in 1982 and 1984, respectively, both in electrical engineering.

From 1984 to 1987, he worked in Electrical Engineering Department, Beijing Institute of Technology as a faculty member, where his research dealt mainly with the Six-Port Measurement Techniques. Presently, he is a graduate in Electrical Engineering Department, University of Maryland at College Park, working towards the Ph.D. degree. His research interests are in the area of modeling microwave and millimeter-wave waveguides, devices and circuits.

Kawthar A. Zaki (SM'85–F'91) received the B.S. degree with honors from Ain Shams University, Cairo, Egypt, in 1962, and the M.S. and Ph.D. degrees from the University of California, Berkeley, in 1966 and 1969, respectively, all in electrical engineering.

From 1962 to 1964, she was a Lecturer in the Department of Electrical Engineering, Ain Shams University. From 1965 to 1969, she held the position of Research Assistant in the Electronic Research Laboratory, University of California, Berkeley. She joined the Electrical Engineering Department, University of Maryland, College Park, MD, in 1970, where she is presently Professor of Electrical Engineering. Her research interests are in the areas of electromagnetics, microwave circuits, optimization, computer-aided design, and optically controlled microwave and millimeter wave devices.

Ali E. Atia (S'67–M'69–SM'78–F'87) received the B.S. degree from Ain Shams University, Cairo, Egypt, in 1962, and the M.S. and Ph.D. degrees from the University of California, Berkeley, in 1966 and 1969, respectively, all in electrical engineering.

Prior to joining COMSAT in 1969, he held various research and teaching positions at both these universities. As a Senior Scientist in the Microwave Laboratory at COMSAT Laboratories, he has made original contributions to satellite transponder and antenna technologies, most notably the development of the dual-mode microwave filters technology. He has also made significant contributions to several satellite programs, including INTELSAT IV-A, V, V-A, VI, and ARABSAT. He was responsible for the design, implementation, qualification, and testing of major subsystems in COMSAT's NASA ATS-F propagation experiment and the COMSTAR Ka-band beacon experiment. As Senior Director in COMSAT Systems Division he was responsible for communications systems design, integration, implementation, and testing under contracts with various government and commercial customers. Presently he is Vice President and Chief Engineer for COMSAT Systems Division, Clarksburg, MD.

Dr. Atia is an Associate Fellow of the AIAA and a Member of Sigma Xi.